

# Three-dimensional flows in slowly-varying planar geometries

Eric Lauga<sup>1</sup>, Abraham D. Stroock<sup>2</sup> and Howard A. Stone<sup>1</sup>

<sup>1</sup>*Division of Engineering and Applied Sciences,  
Harvard University, Cambridge, MA 02138,*

<sup>2</sup>*School of Chemical and Biomolecular Engineering,  
Cornell University, Ithaca, NY 14853.*

(Dated: June 12, 2018)

## Abstract

We consider laminar flow in channels constrained geometrically to remain between two parallel planes; this geometry is typical of microchannels obtained with a single step by current microfabrication techniques. For pressure-driven Stokes flow in this geometry and assuming that the channel dimensions change slowly in the streamwise direction, we show that the velocity component perpendicular to the constraint plane cannot be zero unless the channel has both constant curvature and constant cross-sectional width. This result implies that it is, in principle, possible to design “planar mixers”, *i.e.* passive mixers for channels that are constrained to lie in a flat layer using only streamwise variations of their in-plane dimensions. Numerical results are presented for the case of a channel with sinusoidally varying width.

## I. INTRODUCTION

The rapid development of microfluidic systems and their applications in domains such as aeronautics, chemistry, material synthesis, medical diagnostics and drug delivery has recently motivated investigations of new research questions in fluid dynamics at small scales ([1, 2, 3]). A particularly active research area is the design of mixers for microdevices. This task has proven itself to be a real engineering challenge due to a variety of physical and practical constraints. Physically, the typical cross-sectional dimensions of microchannels in current microfluidic systems are on the order of  $10 - 100 \mu\text{m}$  ([2, 4]). On this scale, practical flows of common liquids ( $U \approx 0.1 - 10 \text{ cm/s}$ ) have low Reynolds numbers,  $Re < 10$ , and turbulent mixing of the fluid does not generally occur. At the same time, the Peclet number for mass transfer in these flows, defined as the ratio of a typical diffusive time to a typical advection time is high,  $Pe > 100$ , and purely diffusive mixing across the flow is slow. For applications that require mixing, it is therefore necessary to design channels that will lead to efficient convective mixing.

In a channel geometry, the strongest gradients of concentration are typically oriented in a direction normal to the principal axis of the channel, because the gradients exist between co-flowing streams of distinct chemical makeup. An effective mixing flow in a channel must therefore stir the fluid over the cross-section with transverse flows as the fluid progresses downstream in the axial flow; such a flow must possess three non-zero components. An effective stirring flow rapidly folds the fluid into itself so as to decrease the distance that diffusion must act to homogenize concentrations. The potential of a given channel-flow to mix efficiently can be judged by several characteristics: (1) the ratio of the transverse to the axial velocities. If this ratio is too small, then the axial length of channel required for mixing is likely to be impractically long, regardless of the detailed character of the flow; (2) the distribution of transverse flows within the cross-section of the channel. If the flows are confined to small areas within the cross-section, then they will be ineffective at exchanging fluid between these areas and with areas in which no flow exists. (3) the evolution of the transverse flows as a function of axial position along the channel. An efficient mixer should produce Lagrangian chaos; in particular, no streamwise symmetries should be present [5]. This feature is achieved in a channel-geometry when the position and orientation of transverse flows vary axially such that all fluid elements travelling in the channel experience an alternating sequence of rotational and extensional flows

([6]).

In designing a laminar mixer for microfluidic applications, it is also important to take into account the constraints imposed by technology and conservation laws. Designs of mixers should be scalable to smaller systems, resistant to fouling by particulate matter, and efficient with respect to power consumption. Moreover, the typical lithographic processes currently used in microfabrication lead to planar geometries.

A variety of active ([7, 8]) and passive ([9, 10, 11, 12, 13]) methods have recently been proposed to generate stirring flows for mixing purposes. All of the passive designs that have been demonstrated to be effective rely however on multilayer or non-planar structures in order to generate three-dimensional flows. A single lithographic step generates a single flat layer of structure with horizontal top and bottom walls and (relatively) vertical side walls (see Figure 1) ([14]). More complicated structures, e.g. a non-intersecting cross-over between two channels, require multiple lithographic steps, with spatial alignment between each layer of structure. Each added layer of structure increases the difficulty of fabrication and complicates scaling down to smaller devices.

Motivated by such practical considerations in this paper, we will be interested in characterizing the potential for mixing of the simplest planar geometrical configurations obtained in a single fabrication step. Two such geometries are illustrated in Figure 1. Suppose we fabricate a channel constrained between two parallel planes of constant separation, can such a configuration mix? In order to be able to give an answer to this question that is robust to change in flow conditions, we will assume zero Reynolds number flows in the channel. This assumption also implies that our conclusions will remain valid in smaller flow systems of the same design.

It is known that the steady-state velocity field in a straight channel of constant rectangular cross section is unidirectional ([15]) and therefore cannot mix except by molecular diffusion; similarly, the velocity field in a curved channel of constant cross-section and constant curvature is unidirectional ([16])[27]. As a consequence, the simplest potential design for a *steady-state* mixer for Stokes flow is that of a channel with variations of shape, that include changes of both curvature and cross-sectional dimensions in the streamwise direction.

In order for flow in such a channel to potentially mix by advection in the three dimensions of the channel, the velocity field needs three non-zero components. While it is clear that these variations in shape will lead to non-zero in-plane components of the velocity, as would also

be the case in a truly two-dimensional channel, it is not obvious that the (third) out-of-plane component will *always* be non-zero. We ask therefore the following question: *under which circumstances is the out-of-plane component of the velocity field always non-zero?* And in this case, what is the expected magnitude of the vertical flow?

The flows in a circular pipe of varying cross-section ([17]) or varying small curvature ([18]) have been studied and three-dimensional flow is obtained at zero Reynolds number. However, because the equation for the shape of a circular pipe couples the two directions that are perpendicular to its axis of symmetry, these results cannot be applied to the flow in a planar geometry and a separate analysis has to be carried out. Recently, Balsa [19] studied the secondary flow in a Hele-Shaw cell in which a vertical cylinder is immersed, at Reynolds number unity based on the cylinder length, and showed the presence of streamwise vorticity in a boundary layer on the cylinder surface; an earlier study by Thompson [20] focused on viscous features.

The geometry of a generic microchannel constrained between two parallel planes with fixed separation and with no obstacles is illustrated in Figure 1 (top). The shape of the channel can be entirely described by two degrees of freedom: (1) the shape of its centerline plane and (2) the local symmetric width of the channel around this centerline. We will consider in this paper the consequences of both and will treat each of them separately for simplicity.

The paper is organized as follows. In section II A we consider the case of a straight channel with varying cross section in the direction perpendicular to both the flow and the constraint plane and in section II B we consider the case of a curved channel of constant cross section but varying curvature. In both cases, under the assumption of an arbitrary but slowly varying cross section and curvature respectively, we show that the velocity component perpendicular to the constraint plane cannot be zero unless cross-section and curvature are both constant, and therefore the flow is fully three-dimensional in all other cases. We apply these results in section III where we calculate the leading-order velocity field in the case of a straight channel of varying cross section and illustrate the flow patterns on a sinusoidally varying channel. We conclude in section IV with a discussion of both the practical advantages and limitations that these results imply for mixing design. Appendices A 1 and A 2 present proofs for some of the results used in sections II A and II B respectively and Appendix B presents the calculation for the leading-order velocity field in the case of a channel of arbitrary shape.

## II. THREE-DIMENSIONALITY OF THE FLOW

### A. Straight microchannel of varying cross section

In this section we consider the case of a straight microchannel of varying cross section, as illustrated in Figure 2. A pressure-driven flow takes place in the  $x$  direction of a channel of constant height  $2h$  in the  $z$ -direction and varying width  $2hf(x/\lambda)$  in the  $y$  direction, where  $\lambda$  is the axial length scale on which such variations occur. The equations of motion and mass conservation for an incompressible Stokes flow are written

$$\nabla p = \mu \nabla^2 \mathbf{u}, \quad \nabla \cdot \mathbf{u} = 0 \quad (1)$$

with the no-slip boundary condition  $\mathbf{u}(x, y = \pm hf(x/\lambda), z) = \mathbf{u}(x, y, z = \pm h) = \mathbf{0}$ , on the four bounding surfaces. The flow rate  $Q$  is set by upstream conditions and is constant

$$\int_{-h}^h \int_{-hf(x/\lambda)}^{+hf(x/\lambda)} (\mathbf{u} \cdot \mathbf{e}_x) dy dz = Q. \quad (2)$$

We now make the assumption that the width of the channel is slowly varying. If we define  $\epsilon = h/\lambda$ , this assumption is equivalent to assuming that  $\epsilon \ll 1$ . Using the notations  $\mathbf{u} = (u, v, w)$  for the velocity field, we can now nondimensionalize the previous set of equations (1)-(2) by scaling lengths, velocities and pressure by

$$(x, y, z) = (\lambda \tilde{x}, h \tilde{y}, h \tilde{z}), \quad (u, v, w) = \frac{Q}{h^2} (\tilde{u}, \epsilon \tilde{v}, \epsilon \tilde{w}), \quad p = \frac{\lambda \mu Q}{h^4} \tilde{p}. \quad (3)$$

Dropping the tildes in the dimensionless variables for convenience, the dimensionless Stokes equation is

$$\nabla p = \left( \epsilon^2 \frac{\partial^2}{\partial x^2} + \frac{\partial^2}{\partial y^2} + \frac{\partial^2}{\partial z^2} \right) [u, \epsilon^2 v, \epsilon^2 w] \quad (4)$$

and the dimensionless continuity equation is

$$\frac{\partial u}{\partial x} + \frac{\partial v}{\partial y} + \frac{\partial w}{\partial z} = 0. \quad (5)$$

We look for a regular perturbation expansion for both the velocity and pressure fields under the form

$$(u, v, w, p) = (u_0, v_0, w_0, p_0) + \epsilon^2 (u_2, v_2, w_2, p_2) + \mathcal{O}(\epsilon^4) \quad (6)$$

which is usual in lubrication theory (see e.g. [21]). The leading-order  $\mathcal{O}(\epsilon^0)$  term of Stokes equation (1) is given by

$$\frac{\partial p_0}{\partial x} = \left( \frac{\partial^2}{\partial y^2} + \frac{\partial^2}{\partial z^2} \right) u_0, \quad \frac{\partial p_0}{\partial y} = \frac{\partial p_0}{\partial z} = 0 \quad (7)$$

subject to the no-slip boundary condition  $u_0(x, y = \pm f(x), z) = u_0(x, y, z = \pm 1) = 0$ , and constant flow rate

$$4 \int_0^1 \int_0^{f(x)} u_0 \, dy \, dz = 1. \quad (8)$$

The axial velocity  $u_0$  is then easily calculated by separation of variables ([15])

$$u_0(x, y, z) = \frac{1}{2} \frac{dp_0}{dx} \left\{ (z^2 - 1) + \sum_{n \geq 0} \frac{4(-1)^n}{k_n^3} \left( \frac{\cosh k_n y}{\cosh k_n f(x)} \right) \cos k_n z \right\} \quad (9)$$

with  $k_n = (n + \frac{1}{2})\pi$ . This solution is simply the axial Poiseuille velocity in a straight channel of constant cross section evaluated at each location along the channel. The leading-order axial pressure gradient is then given by the flow rate condition (8) which leads to

$$\frac{dp_0}{dx} = \frac{3}{4f(x)} \left\{ \frac{6}{f(x)} \sum_{n \geq 0} \frac{\tanh(k_n f(x))}{k_n^5} - 1 \right\}^{-1}. \quad (10)$$

Note that (4) and (5) show that at next order in  $\epsilon^2$ , the leading-order out of plane velocity field  $(v_0, w_0)$  satisfies a two-dimensional Stokes equation with an effective distribution of mass sources and sinks given by  $-du_0/dx$ . Let us now assume these sources and sinks lead to a planar velocity field is planar in the sense that the component of the velocity perpendicular to the constraint plane is zero,  $w_0 = 0$ . In this case, the continuity equation from (1) is written

$$\frac{\partial u_0}{\partial x} + \frac{\partial v_0}{\partial y} = 0, \quad (11)$$

and allows us to solve explicitly for the  $y$ -component of the velocity  $v_0$ . Using the fact that  $u_0$  satisfies the no-slip condition on the walls of the channels, it is straightforward to obtain that  $v_0$  is given by

$$v_0(x, y, z) = \frac{\partial}{\partial x} \int_{-f(x)}^y u_0(x, y', z) \, dy'. \quad (12)$$

The solution (12) satisfies the no-slip conditions for  $v_0$  at  $z = \pm 1$  and  $y = -f(x)$ . If it also satisfies the remaining no-slip condition at  $y = f(x)$  then the leading-order solution would be

entirely characterized and the flow would be planar at leading-order. The condition at  $y = f(x)$  will however be satisfied if and only if

$$\frac{\partial}{\partial x} \int_{-f(x)}^{f(x)} u_0(x, y', z) dy' = 0 \quad (13)$$

for all values of  $x$  and  $z$  in the channel. Using the solution (9), (13) can be integrated once to get

$$\frac{dp_0}{dx} \left\{ \sum_{n \geq 0} \frac{(-1)^n}{k_n^4} (\tanh(k_n f(x)) - k_n) \cos k_n z \right\} = \Phi(z). \quad (14)$$

In order for equation (14) to be satisfied for all  $|z| \leq 1$  and  $x \geq 0$ , it is then necessary that for all  $n \geq 0$ ,

$$\frac{dp_0}{dx} (\tanh(k_n f(x)) - k_n) = \delta_n \quad (15)$$

where the  $\{\delta_n\}$  are constants independent of  $x$ . As is shown in Appendix A 1, this can only be true if  $f(x)$  is constant, *i.e.* if the channel cross section is constant. As a consequence, the vertical component of the velocity field  $w_0$  cannot be zero unless the cross section of the channel is constant, in which case  $v_0 = w_0 = 0$ . When this is not the case and the cross section is changing along the channel, then the two-dimensional solution (9)-(12) is inconsistent and the velocity field is fully three-dimensional at this order.

## B. Channel of constant cross section with varying curvature

We now proceed in the same manner as in section II A for the case of the channel of constant cross section but varying curvature, as illustrated in Figure 3. A pressure-driven flow takes place in the axial direction, denoted as  $s$ , of a channel of constant height  $2h$  in the  $z$ -direction and constant width  $2d$  in the third direction, denoted as  $n$  for “normal”. The centerline of the channel is not straight but curved with local radius of curvature  $R(s) = R_0 f(s/\lambda)$  in the orthogonal  $(\mathbf{e}_n, \mathbf{e}_s, \mathbf{e}_z)$  frame, where  $\lambda$  is the typical length scale along the channel on which this local curvature changes. In this geometry, and using the notations  $\mathbf{u} = (u, v, w)$  for the velocity field, it is possible after some algebra to write the dimensional Stokes equation (1) under the

form

$$\begin{aligned} \frac{1}{\mu} \frac{R(s)}{R(s)+n} \frac{\partial p}{\partial s} &= \frac{\partial^2 u}{\partial z^2} + \left( \frac{R(s)}{R(s)+n} \right)^2 \frac{\partial^2 u}{\partial s^2} + \frac{\partial}{\partial n} \left( \frac{1}{R(s)+n} \frac{\partial}{\partial n} (R(s)+n)u \right) \\ &\quad + \frac{2R(s)}{(R(s)+n)^2} \frac{\partial v}{\partial s} + \frac{R(s)}{(R(s)+n)^2} \frac{\partial v}{\partial n} \frac{dR}{ds}, \end{aligned} \quad (16a)$$

$$\begin{aligned} \frac{1}{\mu} \frac{\partial p}{\partial n} &= \frac{\partial^2 v}{\partial z^2} + \left( \frac{R(s)}{R(s)+n} \right)^2 \frac{\partial^2 v}{\partial s^2} + \frac{\partial}{\partial n} \left( \frac{1}{R(s)+n} \frac{\partial}{\partial n} (R(s)+n)v \right) \\ &\quad - \frac{2R(s)}{(R(s)+n)^2} \frac{\partial u}{\partial s} + \frac{R(s)}{(R(s)+n)^3} \frac{dR}{ds} \left( n \frac{\partial v}{\partial s} - u \right), \end{aligned} \quad (16b)$$

$$\begin{aligned} \frac{1}{\mu} \frac{\partial p}{\partial z} &= \frac{\partial^2 w}{\partial z^2} + \left( \frac{R(s)}{R(s)+n} \right)^2 \frac{\partial^2 w}{\partial s^2} + \frac{1}{R(s)+n} \frac{\partial}{\partial n} \left( (R(s)+n) \frac{\partial w}{\partial n} \right) \\ &\quad + \frac{nR(s)}{(R(s)+n)^3} \frac{dR}{ds} \frac{\partial w}{\partial s}, \end{aligned} \quad (16c)$$

and the continuity equation is written

$$\left( \frac{R(s)}{R(s)+n} \right) \frac{\partial u}{\partial s} + \frac{1}{R(s)+n} \frac{\partial}{\partial n} ((R(s)+n)v) + \frac{\partial w}{\partial z} = 0. \quad (17)$$

The two sets of equations (16) and (17) are associated with the no-slip boundary condition on the walls of the channel  $\mathbf{u}(s, n = \pm d, z) = \mathbf{u}(s, n, z = \pm h) = 0$ , as well as with the condition of constant flow rate along the channel

$$\int_{-h}^h \int_{-d}^d (\mathbf{u} \cdot \mathbf{e}_s) dz dn = Q. \quad (18)$$

As in section II A, we now assume a slowly varying curvature, *i.e.* we assume that both  $h/\lambda \ll 1$  and  $d/\lambda \ll 1$ . Equations (16) - (18) can be nondimensionalized by scaling lengths, velocities and pressure by

$$(s, n, z) \sim (\lambda \tilde{s}, d \tilde{n}, h \tilde{z}), \quad (u, v, w) = \frac{Q}{hd} (\tilde{u}, \frac{\epsilon}{\alpha} \tilde{v}, \epsilon \tilde{w}), \quad p = \frac{\lambda \mu Q}{h^3 d} \tilde{p} \quad (19)$$

where we denoted the aspect ratio  $\alpha = h/d = \mathcal{O}(1)$ . Defining  $\beta = d/R_0$  and  $\epsilon = h/\lambda \ll 1$ , and dropping the tildes in the dimensionless variables for convenience, the dimensionless Stokes



equation is

$$\begin{aligned} \frac{f(s)}{f(s) + \beta n} \frac{\partial p}{\partial s} &= \frac{\partial^2 u}{\partial z^2} + \epsilon^2 \left( \frac{f(s)}{f(s) + \beta n} \right)^2 \frac{\partial^2 u}{\partial s^2} + \frac{\partial}{\partial n} \left( \frac{\alpha^2}{f(s) + \beta n} \frac{\partial}{\partial n} (f(s) + \beta n) u \right) \\ &\quad + \frac{2\epsilon^2 \beta f(s)}{(f(s) + \beta n)^2} \frac{\partial v}{\partial s} + \frac{\epsilon^2 f(s) f'(s)}{(f(s) + \beta n)^2} \frac{\partial v}{\partial n}, \end{aligned} \quad (20a)$$

$$\begin{aligned} \frac{\partial p}{\partial n} &= \frac{\epsilon^2}{\alpha^2} \frac{\partial^2 v}{\partial z^2} + \frac{\epsilon^4}{\alpha^2} \left( \frac{f(s)}{f(s) + \beta n} \right)^2 \frac{\partial^2 v}{\partial s^2} + \epsilon^2 \frac{\partial}{\partial n} \left( \frac{1}{f(s) + \beta n} \frac{\partial}{\partial n} (f(s) + \beta n) v \right) \\ &\quad - \frac{2\epsilon^2 \beta f(s)}{(f(s) + \beta n)^2} \frac{\partial u}{\partial s} + \frac{\epsilon^3 \beta f(s) f'(s)}{\alpha (f(s) + \beta n)^3} \left( n \frac{\epsilon}{\alpha} \frac{\partial v}{\partial s} - u \right), \end{aligned} \quad (20b)$$

$$\begin{aligned} \frac{\partial p}{\partial z} &= \epsilon^2 \frac{\partial^2 w}{\partial z^2} + \epsilon^4 \left( \frac{f(s)}{f(s) + \beta n} \right)^2 \frac{\partial^2 w}{\partial s^2} + \frac{\epsilon^2 \alpha^2}{f(s) + \beta n} \frac{\partial}{\partial n} \left( (f(s) + \beta n) \frac{\partial w}{\partial n} \right) \\ &\quad + \frac{n \epsilon^4 \beta f(s) f'(s)}{(f(s) + \beta n)^3} \frac{\partial w}{\partial s}, \end{aligned} \quad (20c)$$

and the dimensionless continuity equation

$$\frac{f(s)}{f(s) + \beta n} \frac{\partial u}{\partial s} + \frac{1}{f(s) + \beta n} \frac{\partial}{\partial n} (f(s) + \beta n) v + \frac{\partial w}{\partial z} = 0. \quad (21)$$

Note that  $\beta$  is not necessary small in actual MEMS applications [22]. We then look for a regular perturbation expansion for both the dimensionless velocity and pressure fields under the form

$$(u, v, w, p) = (u_0, v_0, w_0, p_0) + \epsilon^2 (u_2, v_2, w_2, p_2) + \mathcal{O}(\epsilon^4). \quad (22)$$

The leading-order  $\mathcal{O}(\epsilon^0)$  of the Stokes equation (16) is

$$\frac{f(s)}{f(s) + \beta n} \frac{\partial p_0}{\partial s} = \frac{\partial^2 u_0}{\partial z^2} + \frac{\partial}{\partial n} \left( \frac{\alpha^2}{f(s) + \beta n} \frac{\partial}{\partial n} (f(s) + \beta n) u_0 \right) \quad (23a)$$

$$\frac{\partial p_0}{\partial n} = \frac{\partial p_0}{\partial z} = 0 \quad (23b)$$

together with the no-slip boundary condition  $u_0(s, n = \pm 1, z) = u_0(s, n, z = \pm 1) = 0$ , and constant flow rate

$$\int_{-1}^1 \int_{-1}^1 u_0 \, dz \, dn = 1. \quad (24)$$

Using separation of variables, it is possible to solve for the axial velocity component in equations (23) - (24), similarly to what was done by Rieger & Šesták (1973) for the case of a curved rectangular channel of constant curvature. We obtain

$$u_0(s, n, z) = f(s) \frac{dp_0}{ds} \left\{ \frac{z^2 - 1}{2(f(s) + \beta n)} + \sum_{n \geq 0} U_n \left( \frac{k_n(f(s) + \beta n)}{\alpha \beta} \right) \cos k_n z \right\}, \quad (25)$$

where the set of functions  $U_n$  are defined by

$$U_n(\eta) = E_n(s)K_1(\eta) + F_n(s)I_1(\eta), \quad (26)$$

with  $I_1$  and  $K_1$  as the order-one modified Bessel functions of the first and second kind respectively, and with

$$E_n(s) = \{(f(s) - \beta)I_1(k_n^-(s)) - (f(s) + \beta)I_1(k_n^+(s))\} G_n(s), \quad (27a)$$

$$F_n(s) = \{(f(s) + \beta)K_1(k_n^+(s)) - (f(s) - \beta)K_1(k_n^-(s))\} G_n(s) \quad (27b)$$

where

$$G_n(s) = \frac{2(-1)^n}{k_n^3(f(s)^2 - \beta^2)} \{I_1(k_n^-(s))K_1(k_n^+(s)) - I_1(k_n^+(s))K_1(k_n^-(s))\}^{-1}, \quad (28)$$

and

$$k_n^\pm(s) = \frac{k_n(f(s) \pm \beta)}{\alpha\beta}. \quad (29)$$

Using the identities  $K'_0 = -K_1$  and  $I'_0 = -I_1$  and the flow rate condition (24) we obtain the pressure gradient

$$\frac{dp_0}{ds} = \frac{1}{2f(s)} \left\{ \alpha \sum_{n \geq 0} (-1)^n \frac{H_n(s)}{k_n^2} - \frac{1}{3\beta} \ln \left( \frac{f(s) + \beta}{f(s) - \beta} \right) \right\}^{-1}, \quad (30)$$

with

$$H_n(s) = E_n(s) \{K_0(k_n^-(s)) - K_0(k_n^+(s))\} + F_n(s) \{I_0(k_n^+(s)) - I_0(k_n^-(s))\}. \quad (31)$$

As in section II A, let us now make the assumption that the flow is planar, *i.e.* that the leading-order vertical component of the velocity field is zero,  $w_0 = 0$ . In this case the continuity equation (17) becomes

$$\frac{\partial u_0}{\partial s} + \frac{1}{f(s)} \frac{\partial}{\partial n} (f(s) + \beta n) v_0 = 0. \quad (32)$$

which can be used to solved exactly for  $v_0$

$$v_0(s, n, z) = -\frac{f(s)}{f(s) + \beta n} \frac{\partial}{\partial s} \left\{ \int_{-1}^n u_0(t, n', z) dn' \right\}. \quad (33)$$

The solution (33) satisfies the no-slip boundary condition at  $z = \pm 1$  and  $n = -1$ ; if the condition at  $n = 1$  was also satisfied, the leading-order velocity field would be two-dimensional at leading-order,  $w_0 = 0$ . The no-slip boundary condition evaluated at  $n = 1$  will however be satisfied if and only if

$$\frac{\partial}{\partial s} \left\{ \int_{-1}^1 u_0(t, n', z) dn' \right\} = 0, \quad (34)$$

for all values of  $s$  and  $z$ . Using the solution for the axial velocity (25), (34) can be integrated once to obtain

$$f(s) \frac{dp_0}{ds} \left\{ \sum_{n \geq 0} \cos k_n z \left( \frac{\alpha H_n(s)}{k_n} - \frac{2(-1)^n}{\beta k_n^3 \ln \left( \frac{f(s)+\beta}{f(s)-\beta} \right)} \right) \right\} = \Psi(z), \quad (35)$$

where  $H_n$  is defined in (31). In order for (35) to be satisfied for all  $|z| \leq 1$  and  $s \geq 0$ , it is necessary that all for all  $n \geq 0$ ,

$$f(s) \frac{dp_0}{ds} \left\{ \frac{\alpha H_n(s)}{k_n} - \frac{2(-1)^n}{\beta k_n^3 \ln \left( \frac{f(s)+\beta}{f(s)-\beta} \right)} \right\} = \gamma_n \quad (36)$$

where the  $\{\gamma_n\}$  are constants independent of  $s$ . As is shown in Appendix A 2, (36) can be satisfied if and only if  $f(s)$  is constant, *i.e.* if the curvature of the channel is constant, in which case  $v_0 = w_0 = 0$ . When this is not the case and the curvature is changing along the channel, then the two-dimensional solution (25)-(33) is inconsistent and the velocity field is fully three-dimensional at this order.

### III. ILLUSTRATION OF THE THREE-DIMENSIONAL FLOWS

We have demonstrated in the previous two sections that flows in channels constrained to remain in a layer of constant thickness are in general three-dimensional, *i.e.* they possess a non-zero component of the velocity perpendicular to the constraint plane. We illustrate these results in this section for the case studied in section II A of a straight channel of varying width. We calculate the three components of the leading-order velocity field  $(u_0, v_0, w_0)$  and illustrate the flow patterns in a sinusoidally varying channel; the calculation for the general case of an asymmetric channel is more intricate and we present it in Appendix B for the interested reader.

#### A. Governing equations

Because the velocity field  $(u_0, v_0, w_0)$  is three-dimensional, the continuity equation in (1) becomes

$$\frac{\partial u_0}{\partial x} + \frac{\partial v_0}{\partial y} + \frac{\partial w_0}{\partial z} = 0, \quad (37)$$

where  $u_0$  is still given by equation (9). Under Stokes flow conditions, the pressure is harmonic  $\nabla^2 p = 0$ , and therefore the velocity field always satisfies the biharmonic equation  $\nabla^4 \mathbf{u} = 0$ . Consequently, within the lubrication approximation (3) and (6), the  $y$  and  $z$  component of the dimensionless velocity field satisfy

$$\nabla_{\perp}^4 v_0 = 0, \quad \text{where} \quad \nabla_{\perp}^2 \equiv \left( \frac{\partial^2}{\partial y^2} + \frac{\partial^2}{\partial z^2} \right) \quad (38a)$$

$$\nabla_{\perp}^4 w_0 = 0. \quad (38b)$$

Similarly, the vorticity is harmonic  $\nabla^2 \boldsymbol{\omega} = 0$ , so that under the lubrication approximation, its leading-order axial component  $\omega_0 = \frac{\partial w_0}{\partial y} - \frac{\partial v_0}{\partial z}$  satisfies

$$\nabla_{\perp}^2 \omega_0 = 0. \quad (39)$$

It is necessary to solve the set of equations (37), (38) and (39) along with the no-slip boundary conditions in order to obtain the final solution for  $(v_0, w_0)$ .

## B. Subset of equations

Let us now show that it is sufficient to solve equations (37) and (38a) to obtain (38b) and (39). Let us suppose (37) and (38a) are satisfied. Evaluating the bi-harmonic  $\nabla_{\perp}^2$  of the continuity equation (37) leads to

$$\frac{\partial}{\partial z} \nabla_{\perp}^4 w_0 = 0 \rightarrow \nabla_{\perp}^4 w_0 = \Gamma(x, y). \quad (40)$$

Because of the symmetries in the configuration illustrated in Figure 1, the solution of Stokes equation has to satisfy  $w_0(x, y, -z) = -w_0(x, y, z)$  (and also  $v_0(x, y, -z) = v_0(x, y, z)$ ). Consequently  $\nabla_{\perp}^4 w_0$  is also odd with respect to  $z$  and necessarily  $\Gamma(x, y) = 0$ , so that equation (38b) is satisfied. In the same fashion, it is straightforward from (37) to obtain

$$\frac{\partial \omega_0}{\partial z} = 0 \rightarrow \omega_0 = \Lambda(x, y). \quad (41)$$

Using the fact that  $w_0$  and  $v_0$  are respectively odd and even with respect to  $z$ , it is clear that  $\omega_0$  is odd with respect to  $z$  so that  $\Lambda(x, y) = 0$ . The result of equation (39) is therefore recovered. As a consequence, it is sufficient to solve equations (37) and (38a) to obtain the complete solution for the leading-order velocity field.

### C. Velocity field calculation

To obtain the leading-order solution for the three-dimensional velocity field in the channel, we solve equations (38a) and (37), along with the no-slip boundary conditions for  $v_0$  and  $w_0$  and with the axial velocity  $u_0$  given by (9). In order to do so, we use the technique introduced more than a century ago by Lamé ([23]) to solve planar elasticity problem where biharmonic equations arise (see also the general discussion in [24]). Here we effectively demonstrate that these ideas also apply as well to slowly varying flows. Using the following symmetries in the velocity field

$$v_0(x, y, -z) = v_0(x, y, z), \quad v_0(x, -y, z) = -v_0(x, y, z), \quad (42a)$$

$$w_0(x, -y, z) = w_0(x, y, z), \quad w_0(x, y, -z) = -w_0(x, y, z), \quad (42b)$$

we look for a solution of (38a) under the form of a double Fourier series in  $y$  and  $z$

$$v_0(x, y, z) = \sum_{n \geq 0} A_n(x, y) \cos k_n z + \sum_{m > 0} B_m(x, z) \sin \left( \frac{\ell_m y}{f(x)} \right), \quad (43)$$

with  $\ell_m = m\pi$  and  $k_n = (n + 1/2)\pi$ . In order for (38a) and (42a) to be satisfied, the functions  $A_n$  and  $B_m$  are given by [28]

$$A_n(x, y) = a_n(x) P_n(x, y), \quad B_m(x, z) = b_m(x) Q_m(x, z) \quad (44)$$

with

$$P_n(x, y) = f(x) \sinh(k_n y) - y \cosh(k_n y) \tanh(k_n f(x)) \quad (45a)$$

$$Q_m(x, z) = \tanh \left( \frac{\ell_m}{f(x)} \right) \cosh \left( \frac{\ell_m z}{f(x)} \right) - z \sinh \left( \frac{\ell_m z}{f(x)} \right) \quad (45b)$$

and where both  $(a_n(x))$  and  $(b_m(x))$  are unknown functions to be determined. With the axial solution (9) written

$$u_0(x, y, z) = \sum_{n \geq 0} \mathcal{U}_n(x, y) \cos k_n z, \quad \mathcal{U}_n(x, y) = \frac{2(-1)^n}{k_n^3} \frac{dp_0}{dx} \left( \frac{\cosh(k_n y)}{\cosh(k_n f(x))} - 1 \right) \quad (46)$$

and with (43), integration of the continuity equation (37) leads to the third component of the velocity field

$$w_0(x, y, z) = - \sum_{n \geq 0} \frac{1}{k_n} \left( \frac{\partial \mathcal{U}_n}{\partial x} + a_n(x) \frac{\partial P_n}{\partial y} \right) \sin k_n z - \sum_{m > 0} \frac{\ell_m b_m(x) T_m(x, z)}{f(x)} \cos \left( \frac{\ell_m y}{f(x)} \right) \quad (47)$$

with

$$T_m(x, z) = \left( \frac{f(x)}{\ell_m} \tanh \left( \frac{\ell_m}{f(x)} \right) + \frac{f(x)^2}{\ell_m^2} \right) \sinh \left( \frac{\ell_m z}{f(x)} \right) - \frac{f(x)}{\ell_m} z \cosh \left( \frac{\ell_m z}{f(x)} \right). \quad (48)$$

The sets of unknown functions  $(a_n)$  and  $(b_m)$  are finally determined by enforcing the no-slip boundary condition for the solution (47) at both  $z = \pm 1$  and  $y = \pm f(x)$ . As is usually the case for problems involving biharmonic equations (e.g. [24]), the final result involves an infinite system of linear algebraic equations given by

$$\begin{cases} a_n(x) = \overline{a_n}(x) + \sum_{m>0} A_{nm}(x) b_m(x) & (n \geq 0), \\ b_m(x) = \overline{b_m}(x) + \sum_{n \geq 0} B_{mn}(x) a_n(x) & (m > 0), \end{cases} \quad (49)$$

with

$$\overline{a_n}(x) = -\frac{\partial \mathcal{U}_n}{\partial x}(x, f(x)) \left\{ \frac{\partial P_n}{\partial y}(x, f(x)) \right\}^{-1}, \quad (50a)$$

$$A_{nm}(x) = \frac{2(-1)^{m+1} \ell_m k_n}{f(x)} \left\{ \frac{\partial P_n}{\partial y}(x, f(x)) \right\}^{-1} \int_0^1 T_m(x, z) \sin k_n z \, dz, \quad (50b)$$

$$\overline{b_m}(x) = \frac{2}{\ell_m T_m(x, 1)} \sum_{n \geq 0} \frac{(-1)^{n+1}}{k_n} \int_0^f \frac{\partial \mathcal{U}_n}{\partial x}(x, y) \cos \left( \frac{\ell_m y}{f(x)} \right) dy, \quad (50c)$$

$$B_{mn}(x) = \frac{2(-1)^{n+1}}{k_n \ell_m T_m(x, 1)} \int_0^f \frac{\partial P_n}{\partial y}(x, y) \cos \left( \frac{\ell_m y}{f(x)} \right) dy. \quad (50d)$$

Note that, at a given position  $x$ , both the  $(a_n(x))$  and  $(b_n(x))$  are entirely determined by the instantaneous values of  $f(x)$  and  $f'(x)$ ; each subsequent order in the long-wavelength expansion (6) will bring an additional dependance on a higher derivative of  $f(x)$ .

## D. Further calculations

### 1. Axial vorticity

Given the sets of  $\{a_n\}$  and  $\{b_n\}$ , we can evaluate the axial component of the vorticity

$$\omega_0 = \frac{\partial w_0}{\partial y} - \frac{\partial v_0}{\partial z}:$$

$$\omega_0(x, y, z) = - \sum_{n \geq 0} \frac{1}{k_n} \left( \frac{\partial^2 \mathcal{U}_n}{\partial x \partial y} + a_n(x) \frac{\partial^2 P_n}{\partial y^2} - k_n^2 a_n(x) P_n(x, y) \right) \sin k_n z \quad (51a)$$

$$+ \sum_{m > 0} \left( \frac{\ell_m^2 b_m(x) T_m(x, z)}{f(x)^2} - b_m(x) \frac{\partial Q_m}{\partial z} \right) \sin \left( \frac{\ell_m y}{f(x)} \right). \quad (51b)$$

## 2. Quadrant-averaged velocities

The quadrant-averaged velocities can also be evaluated, for example in the quadrant ( $y > 0, z > 0$ ). The flow rate condition (8) leads to a constant average axial velocity,  $\langle u_0 \rangle(x) = 1/4$ . Integration of (43) and (47) across the quadrant leads to

$$\langle v_0 \rangle(x) = \sum_{n \geq 0} \frac{(-1)^n a_n}{k_n f(x)} \int_0^{f(x)} P_n(x, y) dy + \sum_{m > 0} \frac{b_m f(x)(1 + (-1)^{m+1})}{\ell_m} \int_0^1 Q_m(x, z) dz, \quad (52)$$

and

$$\langle w_0 \rangle(x) = \sum_{n \geq 0} \frac{2(-1)^{n+1}}{k_n^6 f(x)} \frac{d}{dx} \left[ \frac{dp_0}{dx} (\tanh(k_n f(x)) - k_n f(x)) \right]. \quad (53)$$

### E. Case of a sinusoidally varying wall

We chose to illustrate the flow patterns in the case where the wall shape is described by the dimensionless function  $f(x) = 1 + 0.7 \sin x$ ; recall that the actual dimensional wall shape is described by  $f(\epsilon x)$  where  $\epsilon = h/\lambda$ . The infinite system of linear equations (49) was solved numerically by truncating it at finite values of  $n$  and  $m$ . The integrals in (50) only involve linear and trigonometric functions and are evaluated exactly. Note that apart from the system (49), summations are also involved in equations (10) for the pressure gradient and (50c) for  $\overline{b_m}(x)$ , and they also require numerical truncations.

For each case, numerical results were obtained, the truncation was refined and the results were found to converge quickly to a final solution. The truncations at  $n = 50$  in equations (10) and (50c) were found to be suitable to obtain the final solution. Further, a truncation at  $n = m = 20$  in the infinite set of linear equations equation (49) was also found to be appropriate to resolve the flow fields, with results essentially unchanged for higher truncation numbers.

Such techniques allow us to obtain everywhere in space the three leading-order velocity components and therefore, with a simple time advancement scheme, to follow the motion of individual fluid elements and obtain streamlines.

The main results of our flow illustration are displayed in Figures 4, 5 and 6. Figure 4 presents in-plane velocity plots at three locations along the channel direction, as well as iso-value maps at these locations for both in-plane velocity components  $(v_0, w_0)$  and for the axial component of the vorticity  $(\omega_0)$  [29]. Figure 5 displays the flow streamlines along the expansion part of the

channel ( $3\pi/2 < x < 5\pi/2$ ). Finally, Figure 6 displays the maximum cross-sectional as well as average value of the three components ( $u_0, v_0, w_0$ ) of the leading-order dimensionless velocity as a function of the location along the channel centerline.

The numerical results confirm that the flow at leading-order is fully three-dimensional. The plots in Figure 4 allow us to visualize the regions of high and low velocity and vorticity and the streamlines in Figure 5 show the fluid elements are indeed vertically displaced as they are advected along the channel. Note that the similar plots for the contracting part of the channel were not included here as they can be deduced from those in Figure 4 and 5 by symmetry of Stokes's equation.

We also note in Figure 4 that the qualitative picture for the iso-values of  $v_0$  do not vary much between the point of minimum width ( $x = 3\pi/2$ ) and the point of maximum width ( $x = 5\pi/2$ ). In contrast to  $v_0$ , the distribution of vertical velocity  $w_0$  is modified appreciably: it changes from a monotonic variation across the channel (left picture in Figure 4c) to a variation with local minimum/maximum in the middle of the channel and global maximum/minimum near the channel walls (middle and right picture in Figure 4c). Moreover, as can be seen in Figure 4d, the axial vorticity is maximum at the top and bottom walls and decays towards the middle of the channel ( $z=0$ ); the contracting part is therefore the position along the channel where the strongest stirring of material surfaces would occur.

Further, the results of Figure 6 show that under the lubrication approximation, the magnitude of the vertical flow component  $w_0$  decreases monotonically during an expansion ( $3\pi/2 < x < 5\pi/2$ ); by symmetry of Stokes's equation,  $w_0$  increases in a similar fashion during a contraction of the channel, ( $\pi/2 < x < 3\pi/2$ ).

We see also that for the particular case considered here, and within the lubrication approximation, the leading-order  $y$ -component of the velocity  $v_0$  is always about one order of magnitude smaller than the axial component  $u_0$  and that the vertical component  $w_0$  is about one order of magnitude smaller than  $v_0$ ; back to the dimensional variables, these statements become  $v \approx \epsilon u/10$  and  $w \approx \epsilon u/100$ .

Finally, the integrated effect of the vertical flow along the channel length is illustrated in Figure 5 by the vertical deflection of streamlines. The deflection is larger far from the horizontal centerplane (see Figure 5b) and far from the vertical centerplane (see Figure 5a). Over the channel half period, a fluid element on the upper right streamline in Figure 5a experiences a



vertical displacement of about 10% of the channel half-height.

#### IV. CONCLUSION

We have shown in this paper that the only planar channel shapes for which the velocity field is two-dimensional under Stokes flow conditions have both constant curvature and constant cross section (in which case the flow field is in fact unidirectional). In all other cases for the variation of the cross-section and curvature, the velocity is fully three-dimensional at zero Reynolds number and could in principle be used to mix species in simple microdevices that can be manufactured with one step of microfabrication.

A qualitative summary for the occurrence of the third component of the flow can be given using the two-dimensionality condition, *i.e.* equation (13) or (34). The velocity field remains two-dimensional in the channel if the two-dimensional flow rate  $Q(z) = \int u dy$  is constant along the channel for each  $z$ . When this is not the case and  $Q(z)$  is streamwise-dependent, a vertical velocity component is induced by mass conservation. What our study shows is that, under the lubrication approximation, the only channel geometries with no embedded obstacles for which this is not the case are those of both constant width and constant curvature. Note that alternatively, the presence of obstacles such as cylinders in an otherwise straight channel would provide similar geometric features necessary for the occurrence of a three-dimensional flow [20].

As the general form of the continuity equation shows, the magnitude of the ratio of the out-of-plane velocity component  $w$  to the axial component  $u$  scales as the ratio of the cross-sectional length scale  $h$  to the length scale  $\lambda$  over which the variations of the channel geometry occur,

$$\frac{w}{u} \approx \frac{h}{\lambda} = \epsilon. \quad (54)$$

The numerical results presented in section III E for a sinusoidal change in cross-section show that the prefactors for this scaling is about 0.01 for the ratio of the *leading-order* velocity fields  $w_0$  to  $u_0$  and indicate poor mixing. For the case  $h \approx \lambda$ , we could expect however all orders in the perturbation expansion to contribute in a non trivial way, and we expect therefore that with this simple design a vertical flow of strength comparable to the axial flow could exist; if that is not the case and the prefactors for the full calculation are not of order one, the channel will likely present poor mixing characteristics. Note that as the Reynolds number in micromixers

is not exactly zero but can be as high as 100, we also expect in this case the occurrence of non-trivial Dean flow-like contributions to the vertical flow.

We propose to design "planar mixers" by a succession of  $n$  mixing cells of length  $\lambda$  along a single channel. In each cell, we expect the integrated displacements  $\delta y$  and  $\delta z$  of fluid elements in the cross-section, advected by the flow at velocity  $U_{\text{axial}}$ , to be given by

$$\delta y \approx \delta z \approx t_{\perp} U_{\perp}, \quad (55)$$

where  $t_{\perp}$  is the residence time for the flow in the cell  $t_{\perp} \approx \lambda/U_{\text{axial}}$  and  $U_{\perp}$  is the magnitude of the transverse flow, at most  $U_{\perp} \approx hU_{\text{axial}}/\lambda$  so that  $\delta y \approx \delta z \approx h$ . Since the total length of the mixer is  $n\lambda$  and the displacements  $\delta y$  and  $\delta z$  are independent of the cell length, small cells  $\lambda \approx h$  should be chosen. The challenge in the mixing design would then concern (1) the design of each cell, *i.e.* the variations of its radius of curvature and its cross-section, in order to obtain the maximum cross-sectional displacement and (2) the setup of the cell succession in a way that mixing adds up instead of cancelling out; for example the channel studied in section III E would obviously make very poor mixing cells because by symmetry of Stokes flow, every fluid stirring taking place in one part of the channel would be unstirred in the other part of the channel located immediately downstream. In general, good performance may be achieved by avoiding any geometrical symmetry along the streamwise direction.

The calculations presented in this paper assumed slowly varying cross-sectional and curvature change along the channel,  $\epsilon \ll 1$ . As was shown by Lucas (1972) for two-dimensional channels of varying shape, the regular perturbation expansions (6) or (22) are expected to have order one or larger radius of convergence in  $\epsilon$ ; as a consequence, the conclusions reached using the leading-order velocity fields are valid for the entire velocity field when  $\epsilon$  is  $\mathcal{O}(1)$ , and presumably higher even though our results cannot be applied directly. With current microfabrication techniques, the minimum in-plane dimension ( $\approx \lambda$ ) that can be generated is typically greater than the minimum out-of-plane dimension ( $\approx h$ ). As a consequence, the cross-sectional dimensions of microchannels tend to satisfy the criterion,  $\epsilon < 1$ , and the results obtained in this paper are expected to apply for all such cases.

The limitation of the passive mixing strategy proposed here lies in the top-bottom symmetry for the velocity field,  $(u, v, w)(x, y, -z) = (u, v, -w)(x, y, z)$ , due to the symmetries of the Stokes equations. Mixing can therefore not be achieved between the fluids located in the  $z > 0$

and  $z < 0$  planes and consequently, the streams of solutions that are to be mixed must be introduced at the inlet of the channel with alignment in the vertical direction. The case of a straight channel of varying section studied in section II A also possess a right/left symmetry,  $(u, v, w)(x, -y, z) = (u, -v, w)(x, y, z)$ , (see Figure 4) and therefore cannot mix species fluids located in the  $y > 0$  and  $y < 0$  planes. The configuration studied in section II B does not possess such a symmetry and should be used to transport fluid between the  $n > 0$  and  $n < 0$  planes, similarly to what was achieved in Stroock *et al.* (2002). A fully numerical approach to the problem (using e.g. a boundary element method or a commercial code) would allow a detailed study of the proposed mixing design, its optimization, and dispersion characteristics.

## Acknowledgments

The authors acknowledge fruitful discussions with M. Brenner and T. Squires on the subject. We also thank two anonymous referees for useful suggestions. Funding from the Harvard MRSEC and the NSF Division of Mathematical Sciences is gratefully acknowledged.

## APPENDIX A: PROOFS

### 1. Proof of result (15) for straight channels

We show in this section that the only set of width functions  $f(x)$  that satisfy (15) are the constant functions. Let us assume that (15) is satisfied for a function  $f(x)$ . We first rewrite equation (10) for the pressure gradient under the form

$$6 \frac{dp_0}{dx} \sum_{n \geq 0} \frac{\tanh(k_n f(x))}{k_n^5} - f(x) \frac{dp_0}{dx} = \frac{3}{4}. \quad (\text{A1})$$

We then rewrite the condition (15) for two-dimensionality of the flow as

$$\frac{dp_0}{dx} \tanh(k_n f(x)) = \delta_n + k_n \frac{dp_0}{dx} \quad (\text{A2})$$

Substituting the expression obtained in (A2) into (A1) leads to a closed form solution for the axial pressure gradient

$$\frac{dp_0}{dx} = \frac{\Delta_1}{\Delta_2 - f(x)}, \quad \Delta_1 = \frac{3}{4} - 6 \sum_{n \geq 0} \frac{\delta_n}{k_n^5}, \quad \Delta_2 = 6 \sum_{n \geq 0} \frac{1}{k_n^4}. \quad (\text{A3})$$

As a conclusion, the functional form (A3) obtained for the pressure gradient is not consistent with that given by the assumption of the two-dimensionality of the flow (15)

$$\frac{dp_0}{dx} = \frac{\delta_n}{\tanh(k_n f(x)) - k_n}, \quad (\text{A4})$$

unless the function  $f(x)$  is constant.

## 2. Proof of result (36) for curved channels

We show in this section that the only set of curvature functions  $f(s)$  that satisfy (36) are the constant functions. Let us assume that (36) is satisfied for a function  $f(s)$ . We first rewrite equation (30) for the pressure gradient under the form

$$2f(s)\frac{dp_0}{ds} \sum_{n \geq 0} (-1)^n \frac{\alpha H_n(s)}{k_n^2} - \frac{2f(s)}{3\beta} \frac{dp_0}{ds} \ln \left( \frac{f(s) + \beta}{f(s) - \beta} \right) = 1. \quad (\text{A5})$$

We then rewrite the condition (36) for two-dimensionality of the flow as

$$f(s)\frac{dp_0}{ds} \frac{\alpha H_n(s)}{k_n} = \frac{2(-1)^n}{\beta k_n^3 \ln \left( \frac{f(s) + \beta}{f(s) - \beta} \right)} f(s) \frac{dp_0}{ds} + \gamma_n. \quad (\text{A6})$$

Substituting (A6) into (A5) leads to a closed-form solution for the streamwise pressure gradient

$$f(s)\frac{dp_0}{ds} = \frac{\Delta_3 \ln \left( \frac{f(s) + \beta}{f(s) - \beta} \right)}{\ln^2 \left( \frac{f(s) + \beta}{f(s) - \beta} \right) - \Delta_4}, \quad \Delta_3 = 3\beta \left\{ \sum_{n \geq 0} \frac{(-1)^n \gamma_n}{k_n} - \frac{1}{2} \right\}, \quad \Delta_4 = 6 \sum_{n \geq 0} \frac{1}{k_n^4}. \quad (\text{A7})$$

Further, it is possible to use the asymptotic behaviors near  $x \sim \infty$  of Bessel functions (see e.g. [26])  $I_p(x) \sim e^x / \sqrt{2\pi x}$ ,  $K_q(x) \sim \pi e^{-x} / \sqrt{2x}$  to obtain the asymptotic behaviors of  $E_n(s)$ ,  $F_n(s)$ ,  $G_n(s)$  as  $n \rightarrow +\infty$ , from equations (27a), (27b) and (28) respectively. It is then straightforward to obtain the asymptotic behavior of  $H_n$

$$H_n(s) \sim \frac{4(-1)^n f(s)}{k_n^3 (f(s)^2 - \beta^2)}. \quad (\text{A8})$$

This behavior and the condition of two-dimensionality (36) allows to obtain an alternate functional behavior for the streamwise pressure gradient

$$f(s)\frac{dp_0}{ds} \sim \Delta_5 \ln \left( \frac{f(s) + \beta}{f(s) - \beta} \right), \quad \Delta_5 = \frac{\beta k_n^3 (-1)^{n+1} \gamma_n}{2}. \quad (\text{A9})$$

As a conclusion, the two functional forms obtained assuming two-dimensionality of the flow (A7) and (A9) are not consistent with each other unless the function  $f(s)$  is a constant.

## APPENDIX B: LEADING ORDER VELOCITY FIELD FOR ASYMMETRIC WALL PROFILE

We present in this section the solution for the leading-order lubrication velocity field in the case of a planar channel of general shape; the calculation presented here contains that presented in section III C as a special case. We use a cartesian coordinate system, as illustrated in Figure 7. All notations are the same as in section II A, with the difference that the channel is not right/left symmetric and we denote its boundaries by the equations  $y = hf_1(x/\lambda)$  and  $y = -hf_2(x/\lambda)$ , with  $f_1(x) > 0$  and  $f_2(x) > 0$ . Using the same nondimensionalizations and regular expansion as in section II A and defining the convenient notations  $f_1 \triangleq f_1(x)$  and  $f_2 \triangleq f_2(x)$ , we obtain that the leading-order axial velocity field is given by

$$u_0(x, y, z) = \sum_{n \geq 0} \mathcal{U}_n(x, y) \cos k_n z, \quad \mathcal{U}_n(x, y) = 2 \frac{dp_0}{dx} \frac{(-1)^n}{k_n^3} \left\{ \frac{\cosh k_n \left( y + \frac{f_2 - f_1}{2} \right)}{\cosh k_n \left( \frac{f_1 + f_2}{2} \right)} - 1 \right\}, \quad (\text{B1})$$

and a pressure gradient obtained by enforcing the flow rate condition

$$2 \int_0^1 \int_{-f_2}^{f_1} u_0 \, dy \, dz = 1, \quad (\text{B2})$$

which leads to

$$\frac{dp_0}{dx} = \frac{3}{2(f_1 + f_2)} \left\{ \frac{12}{f_1 + f_2} \sum_{n \geq 0} \left( \frac{\tanh \left( k_n \frac{f_1 + f_2}{2} \right)}{k_n^5} \right) - 1 \right\}^{-1}. \quad (\text{B3})$$

Concerning the other two velocity components, the arguments presented in section III B also apply to the configuration considered here and the equations to solve for  $v_0$  and  $w_0$  are equations (38a) and (37), along with the no-slip boundary conditions. Using the top/bottom symmetries in the velocity field

$$v_0(x, y, -z) = v_0(x, y, z), \quad w_0(x, y, -z) = -w_0(x, y, z) \quad (\text{B4})$$

we look for a solution of (38a) under the form of a double Fourier series in  $y$  and  $z$ ,

$$\begin{aligned} v_0(x, y, z) = & \sum_{n \geq 0} A_n(x, y) \cos k_n z + \sum_{m > 0} B_m(x, z) \sin \left( \frac{\ell_m(2y + f_2 - f_1)}{f_1 + f_2} \right) \\ & + \sum_{p \geq 0} C_p(x, z) \cos \left( \frac{k_p(2y + f_2 - f_1)}{f_1 + f_2} \right), \end{aligned} \quad (\text{B5})$$

where  $k_n = (n + 1/2)\pi$ ,  $\ell_m = m\pi$ ,  $k_p = (p + 1/2)\pi$  and

$$A_n(x, y) = a_n(x)P_n(x, y) + b_n(x)Q_n(x, y), \quad (\text{B6a})$$

$$B_m(x, z) = c_m(x)S_m(x, z), \quad (\text{B6b})$$

$$C_p(x, z) = d_p(x)T_p(x, z), \quad (\text{B6c})$$

with

$$P_n(x, y) = (f_1 + f_2) \sinh k_n(f_1 - y) - (f_1 - y) \cosh k_n(f_1 - y) \tanh k_n(f_1 + f_2), \quad (\text{B7a})$$

$$Q_n(x, y) = (f_1 - y) \sinh k_n(f_1 - y) - (f_1 - y) \cosh k_n(f_1 - y) \tanh k_n(f_1 + f_2), \quad (\text{B7b})$$

$$S_m(x, z) = \cosh \left( \frac{2\ell_m z}{f_1 + f_2} \right) - z \frac{\sinh \left( \frac{2\ell_m z}{f_1 + f_2} \right)}{\tanh \left( \frac{2\ell_m}{f_1 + f_2} \right)}, \quad (\text{B7c})$$

$$T_p(x, z) = \cosh \left( \frac{2k_p z}{f_1 + f_2} \right) - z \frac{\sinh \left( \frac{2k_p z}{f_1 + f_2} \right)}{\tanh \left( \frac{2k_p}{f_1 + f_2} \right)}. \quad (\text{B7d})$$

Note that the solution in (B5) satisfies the no-slip boundary condition on all four walls. The integration of the continuity equation (37) leads to the general form of the vertical velocity component

$$\begin{aligned} w_0(x, y, z) = & \sum_{n \geq 0} \left\{ -\frac{1}{k_n} \left( \frac{\partial \mathcal{U}_n}{\partial x} + a_n(x) \frac{\partial P_n}{\partial y} + b_n(x) \frac{\partial Q_n}{\partial y} \right) \right\} \sin k_n z \\ & + \sum_{m > 0} \ell_m c_m(x) Y_m(x, z) \cos \left( \frac{\ell_m(2y + f_2 - f_1)}{f_1 + f_2} \right) \\ & + \sum_{p \geq 0} k_p d_p(x) Z_p(x, z) \sin \left( \frac{k_p(2y + f_2 - f_1)}{f_1 + f_2} \right). \end{aligned} \quad (\text{B8})$$

with

$$Y_m(x, z) = -\frac{1}{\ell_m} \left\{ \left( 1 + \frac{1}{\left( \frac{2\ell_m}{f_1 + f_2} \right) \tanh \left( \frac{2\ell_m}{f_1 + f_2} \right)} \right) \sinh \left( \frac{2\ell_m z}{f_1 + f_2} \right) - \frac{z \cosh \left( \frac{2\ell_m z}{f_1 + f_2} \right)}{\tanh \left( \frac{2\ell_m}{f_1 + f_2} \right)} \right\} \quad (\text{B9a})$$

$$Z_p(x, z) = \frac{1}{k_p} \left\{ \left( 1 + \frac{1}{\left( \frac{2k_p}{f_1 + f_2} \right) \tanh \left( \frac{2k_p}{f_1 + f_2} \right)} \right) \sinh \left( \frac{2k_p z}{f_1 + f_2} \right) - \frac{z \cosh \left( \frac{2k_p z}{f_1 + f_2} \right)}{\tanh \left( \frac{2k_p}{f_1 + f_2} \right)} \right\}. \quad (\text{B9b})$$

The sets of unknown functions  $(a_n)$ ,  $(b_n)$ ,  $(c_n)$  and  $(d_n)$  are finally determined by enforcing the no-slip boundary condition for  $w_0$  in (B8) on the four walls  $z = \pm 1$ ,  $y = f_1$  and  $y = -f_2$ , and

we obtain a set of four infinite linear algebraic equations

$$\left\{ \begin{array}{l} a_i(x) = \overline{a_i}(x) + \sum_{n \geq 0} A_{in}^{(2)}(x)b_n(x) + \sum_{m > 0} A_{im}^{(3)}(x)c_m(x) + \sum_{p \geq 0} A_{ip}^{(4)}(x)d_p(x) \quad (i \geq 0), \\ b_n(x) = \overline{b_n}(x) + \sum_{i \geq 0} B_{ni}^{(1)}(x)a_i(x) + \sum_{m > 0} B_{nm}^{(3)}(x)c_m(x) + \sum_{p \geq 0} B_{np}^{(4)}(x)d_p(x) \quad (n \geq 0), \\ c_m(x) = \overline{c_m}(x) + \sum_{i \geq 0} C_{mi}^{(1)}(x)a_i(x) + \sum_{n \geq 0} C_{mn}^{(2)}(x)b_n(x) + \sum_{p \geq 0} C_{mp}^{(4)}(x)d_p(x) \quad (m > 0), \\ d_p(x) = \overline{d_p}(x) + \sum_{i \geq 0} D_{pi}^{(1)}(x)a_i(x) + \sum_{n \geq 0} D_{pn}^{(2)}(x)b_n(x) + \sum_{m > 0} D_{pm}^{(3)}(x)c_m(x) \quad (p \geq 0), \end{array} \right. \quad (\text{B10})$$

with

$$\overline{a_i}(x) = - \left( \frac{\partial P_i}{\partial y}(x, f_1(x)) \right)^{-1} \frac{\partial u_i}{\partial x}(x, f_1(x)), \quad (\text{B11a})$$

$$\overline{b_n}(x) = - \left( \frac{\partial Q_n}{\partial y}(x, -f_2(x)) \right)^{-1} \frac{\partial \mathcal{U}_n}{\partial x}(x, -f_2(x)), \quad (\text{B11b})$$

$$\overline{c_m}(x) = \frac{2}{\ell_m Y_m(x, 1)(f_1 + f_2)} \left\{ \int_{-f_2}^{f_1} \left( \sum_{j \geq 0} \frac{(-1)^j}{k_j} \frac{\partial u_j}{\partial x}(x, y) \right) \cos \left( \frac{\ell_m(2y + f_2 - f_1)}{f_1 + f_2} \right) dy \right\} \quad (\text{B11c})$$

$$\overline{d_p}(x) = \frac{2}{k_p Z_p(x, 1)(f_1 + f_2)} \left\{ \int_{-f_2}^{f_1} \left( \sum_{j \geq 0} \frac{(-1)^j}{k_j} \frac{\partial u_j}{\partial x}(x, y) \right) \sin \left( \frac{k_p(2y + f_2 - f_1)}{f_1 + f_2} \right) dy \right\} \quad (\text{B11d})$$

and

$$A_{in}^{(2)}(x) = -\delta_{in} \left( \frac{\partial P_i}{\partial y}(x, f_1(x)) \right)^{-1} \frac{\partial Q_i}{\partial y}(x, f_1(x)), \quad (\text{B12a})$$

$$A_{im}^{(3)}(x) = 2(-1)^m k_i \ell_m \left( \frac{\partial P_i}{\partial y}(x, f_1(x)) \right)^{-1} \int_0^1 Y_m(x, z) \sin(k_n z) dz, \quad (\text{B12b})$$

$$A_{ip}^{(4)}(x) = 2(-1)^p k_i k_p \left( \frac{\partial P_i}{\partial y}(x, f_1(x)) \right)^{-1} \int_0^1 Z_p(x, z) \sin(k_n z) dz, \quad (\text{B12c})$$

$$B_{ni}^{(1)}(x) = -\delta_{ni} \left( \frac{\partial Q_n}{\partial y}(x, -f_2(x)) \right)^{-1} \frac{\partial P_n}{\partial y}(x, -f_2(x)), \quad (\text{B12d})$$

$$B_{nm}^{(3)}(x) = 2(-1)^m k_n \ell_m \left( \frac{\partial Q_n}{\partial y}(x, -f_2(x)) \right)^{-1} \int_0^1 Y_m(x, z) \sin(k_n z) dz, \quad (\text{B12e})$$

$$B_{np}^{(4)}(x) = 2(-1)^{p+1} k_n k_p \left( \frac{\partial Q_n}{\partial y}(x, -f_2(x)) \right)^{-1} \int_0^1 Z_p(x, z) \sin(k_n z) dz, \quad (\text{B12f})$$

$$C_{mi}^{(1)}(x) = \frac{2(-1)^i}{k_i \ell_m Y_m(x, 1)(f_1 + f_2)} \int_{-f_2}^{f_1} \frac{\partial P_i}{\partial y}(x, y) \cos\left(\frac{\ell_m(2y + f_2 - f_1)}{f_1 + f_2}\right) dy, \quad (\text{B12g})$$

$$C_{mn}^{(2)}(x) = \frac{2(-1)^n}{k_n \ell_m Y_m(x, 1)(f_1 + f_2)} \int_{-f_2}^{f_1} \frac{\partial Q_n}{\partial y}(x, y) \cos\left(\frac{\ell_m(2y + f_2 - f_1)}{f_1 + f_2}\right) dy, \quad (\text{B12h})$$

$$C_{mp}^{(4)}(x) = \frac{-2k_p Z_p(x, 1)}{\ell_m Y_m(x, 1)(f_1 + f_2)} \int_{-f_2}^{f_1} \cos\left(\frac{\ell_m(2y + f_2 - f_1)}{f_1 + f_2}\right) \sin\left(\frac{k_p(2y + f_2 - f_1)}{f_1 + f_2}\right) dy, \quad (\text{B12i})$$

$$D_{pi}^{(1)}(x) = \frac{2(-1)^i}{k_i k_p Z_p(x, 1)(f_1 + f_2)} \int_{-f_2}^{f_1} \frac{\partial P_i}{\partial y}(x, y) \sin\left(\frac{k_p(2y + f_2 - f_1)}{f_1 + f_2}\right) dy, \quad (\text{B12j})$$

$$D_{pn}^{(2)}(x) = \frac{2(-1)^n}{k_n k_p Z_p(x, 1)(f_1 + f_2)} \int_{-f_2}^{f_1} \frac{\partial Q_n}{\partial y}(x, y) \sin\left(\frac{k_p(2y + f_2 - f_1)}{f_1 + f_2}\right) dy, \quad (\text{B12k})$$

$$D_{pm}^{(3)}(x) = \frac{-2\ell_m Y_m(x, 1)}{k_p Z_p(x, 1)(f_1 + f_2)} \int_{-f_2}^{f_1} \cos\left(\frac{\ell_m(2y + f_2 - f_1)}{f_1 + f_2}\right) \sin\left(\frac{k_p(2y + f_2 - f_1)}{f_1 + f_2}\right) dy, \quad (\text{B12l})$$

Similar numerical technique as the ones illustrated in section III E can be used to solve (B10) and obtain the leading-order velocities in the general case given by (B5) and (B8).

- 
- [1] C.-M. Ho, and Y.-C. Tai “Micro-electro-mechanical systems (MEMS) and fluid flows,” *Ann. Rev. Fluid Mech.* **30**, 579 (1999).
  - [2] G.M. Whitesides and A.D. Stroock “Flexible methods for microfluidics,” *Physics Today* **54**(6), 42, (2001).



- [3] H.A. Stone A.D. Stroock and A. Ajdari “Engineering flows in small devices: Microfluidics towards a lab-on-a-chip,” *Ann. Rev. Fluid Mech.* **36** (to appear) (2004).
- [4] A. Manz, D.J. Harrison, E.M.J. Verpoorte, J.C. Fettinger, H. Ludi and H.M. Widmer “Miniaturization of chemical-analysis systems - a look into next century technology or just a fashionable craze,” *Chimia* **45**(4), 103 (1991).
- [5] I. Mezic and S. Wiggins “On the Integrability and Perturbation of Three-Dimensional Fluid Flows with Symmetry,” *J. Nonlinear Science*, **4**(2), 157 (1994).
- [6] Ottino, J.M. (1990) *The Kinematics of Mixing: Stretching, Chaos and Transport*. Cambridge, Cambridge University Press
- [7] J.C. Rife, M.I. Bell, J.S. Horwitz, M.N. Kabler, R.C.Y. Auyeung and W.J. Kim “Miniature valveless ultrasonic pumps and mixers,” *Sensors and Actuators* **86**, 135 (2000).
- [8] Y.K. Lee, J. Deval, P. Tabeling and C.M. Ho “Chaotic mixing in electrokinetically and pressure driven micro flows,” *Prod IMRET* 5. (2001).
- [9] F.G. Bessoth, A.J. deMello and A. Manz “Microstructure for efficient continuous flow mixing,” *Anal. Commun.* **36**, 213 (1999).
- [10] R.H. Liu, K.V. Sharp, M.G. Olsen, M.A. Stremler, J.G. Santiago, R.J. Adrian, H. Aref and D.J. Beebe “A passive three dimensional ‘C-shape’ helical micromixer,” *J. Microelectromech. Syst.* **9**, 190 (2000).
- [11] A. Bertsch, A. Heimgartner, P. Cousseau, and P. Renaud “Secondary flow in a Hele-Shaw cell,” *Lab-on-a-Chip* **1**, 56 (2001).
- [12] T.J. Johnson, D. Ross, and L.E. Locascio “Rapid microfluidic mixing,” *Anal. Chem* **74**, 45 (2002).
- [13] A.D. Stroock, S.K.W. Dertinger, A. Ajdari, I. Mezic, H.A. Stone and G.M. Whitesides “Chaotic mixer for microchannels,” *Science* **295**, 647 (2002).
- [14] G.T.A. Kovacs *Micromachined transducers sourcebook*. Boston, WCB/McGraw-Hill (1998).
- [15] G.K. Batchelor *An Introduction to Fluid Dynamics*. Cambridge, Cambridge University Press (1967).
- [16] F. Rieger and J. Sesták “Creeping flow of Newtonian fluids in curved rectangular channels,” *App. Sci. Res.* **28**, 89 (1973).
- [17] M.J. Manton “Low Reynolds number flow in slowly varying axisymmetric tubes,” *J. Fluid Mech.*

- 49, 451 (1971).
- [18] S. Murata, Y. Miyake and T. Inaba “Laminar flow in curved pipe with varying curvature,” J. Fluid Mech. **73**, 735 (1976).
  - [19] T.F. Balsa “Secondary flow in a Hele-Shaw cell,” J. Fluid Mech. **372**, 25 (1998).
  - [20] B.W. Thompson “Secondary flow in a Hele-Shaw cell,” J. Fluid Mech. **31**, 379 (1968).
  - [21] S. Ghosal “Lubrication theory for electroosmotic flow in a microfluidic channel of slowly varying cross-section and wall charge,” J. Fluid Mech. **459**, 103 (2002).
  - [22] H. Song, J.D. Tice and R.F. Ismagilov “A Microfluidic System for Controlling Reaction Networks in Time,” Angew. Chem. Int. Edit. **42**(7) 768 (2003).
  - [23] G. Lamé *Leçons sur la théorie mathématiques de l'élasticité des corps solides*. Bachelier, Paris (1852).
  - [24] V.V. Meleshko “Steady Stokes flow in a rectangular cavity,” Proc. Roy. Soc. A **452**, 1999 (1996).
  - [25] R.D. Lucas *A perturbation solution for viscous incompressible flow in channels*. Ph.D. thesis, Stanford University (1972).
  - [26] M. Abramowitz and I.A. Stegun *Handbook of Mathematical Functions*. New-York, Dover Publications (1972).
  - [27] Note that both these results are in fact valid independently of the cross-sectional shape of the channel as long as the shape remains constant. Note also that time-periodic flows in these geometries are also unidirectional and cannot be used for low-Reynolds number mixing (see e.g. the review in [6]).
  - [28] Note that in (44) we use the indices  $n$  and  $m$  twice but do not imply this is an implicit summation notation.
  - [29] Note that the velocity plots in Figure 4a display the two-dimensional  $(y, z)$  secondary flow of a three-dimensional flow, which is not to be confounded with a two-dimensional flow.

## FIGURES

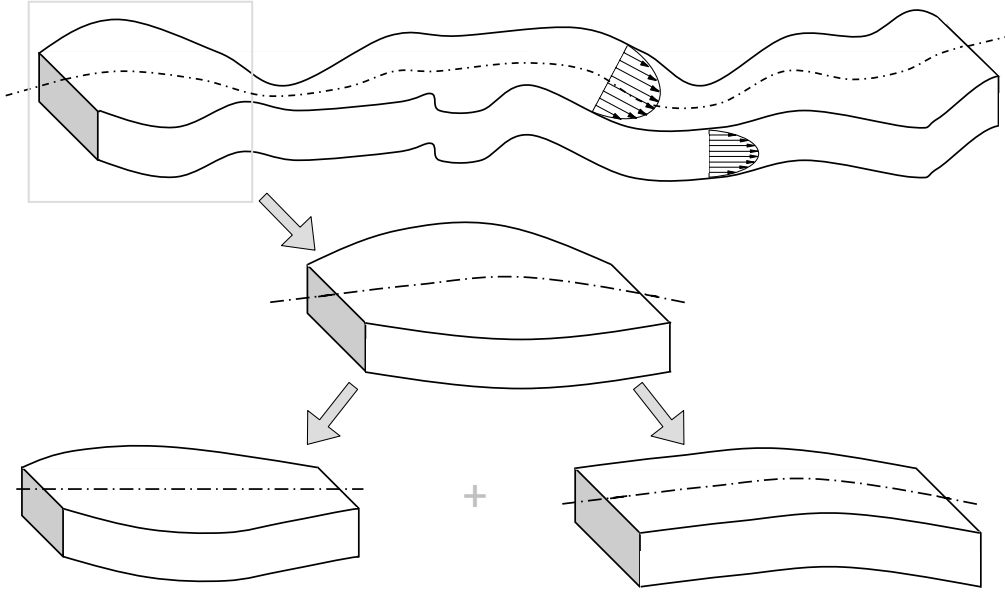


FIG. 1: Generic view of a microchannel constrained to remain between two parallel planes. The design of channel has two degrees of freedom: (1) the shape of its centerline and (2) the relative width of the channel around this centerline.

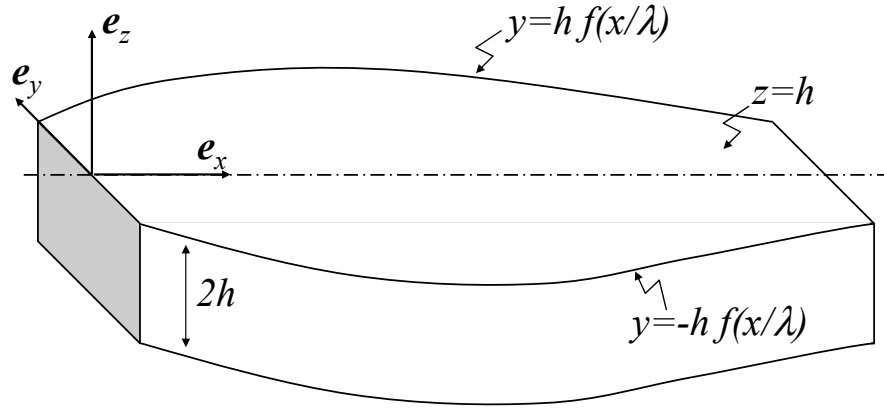


FIG. 2: Straight channel of slowly varying cross section in the  $y$  direction.

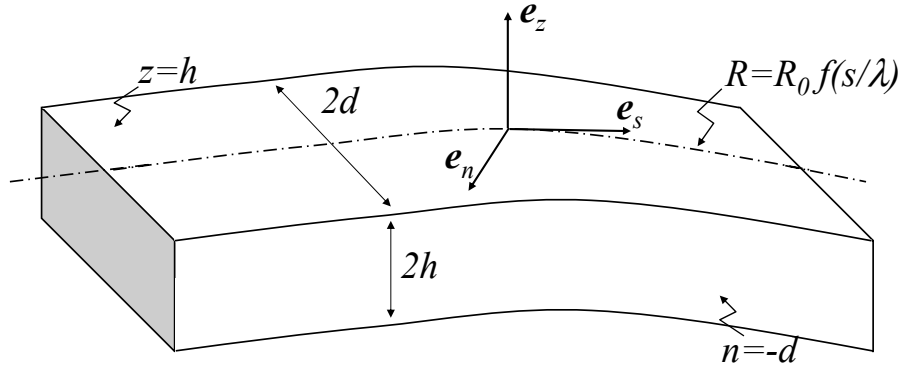


FIG. 3: Curved microchannel of constant cross section and slowly varying planar curvature.

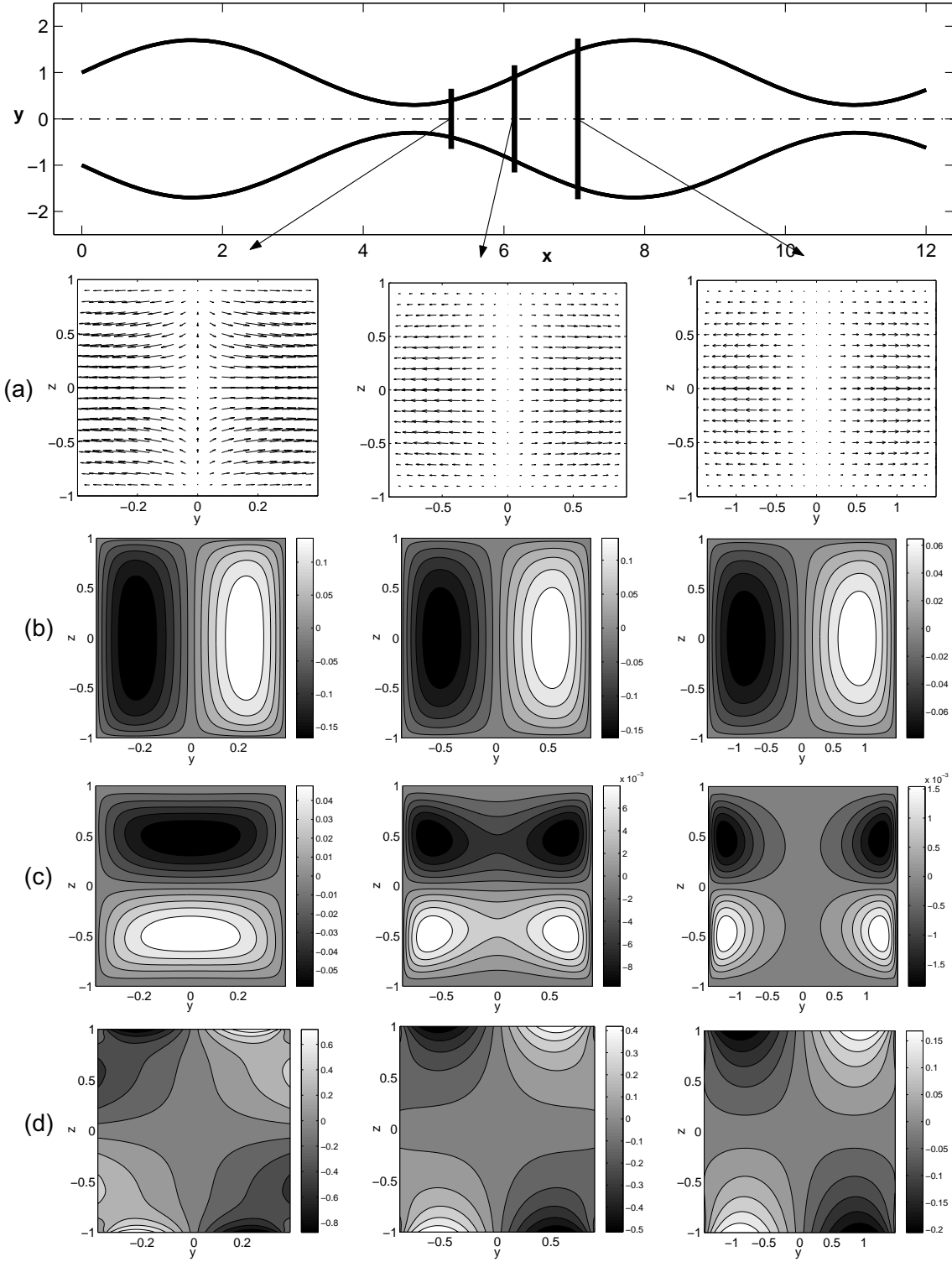


FIG. 4: Illustration of the leading-order three-dimensional flow in the straight planar channel of varying dimensionless cross-section given by  $f(x) = 1 + 0.7 \sin x$ . Top: view the channel. Bottom: plots of the leading-order dimensionless cross-sectional velocity field  $(v_0, w_0)$  and axial vorticity  $\omega_0$  at three locations along the channel:  $x = 5.25, 6.15$  and  $7.05$ ; (a): in-plane velocity plots (the velocities are normalized by their maximum in-plane values); (b): iso-values of the  $y$ -component  $v_0$  of the velocity, from equation (43); (c): iso-values of the  $z$ -component of the velocity  $w_0$ , from equation (47); (d): iso-values of the  $x$ -component of the vorticity  $\omega_0$ , from equation (51).



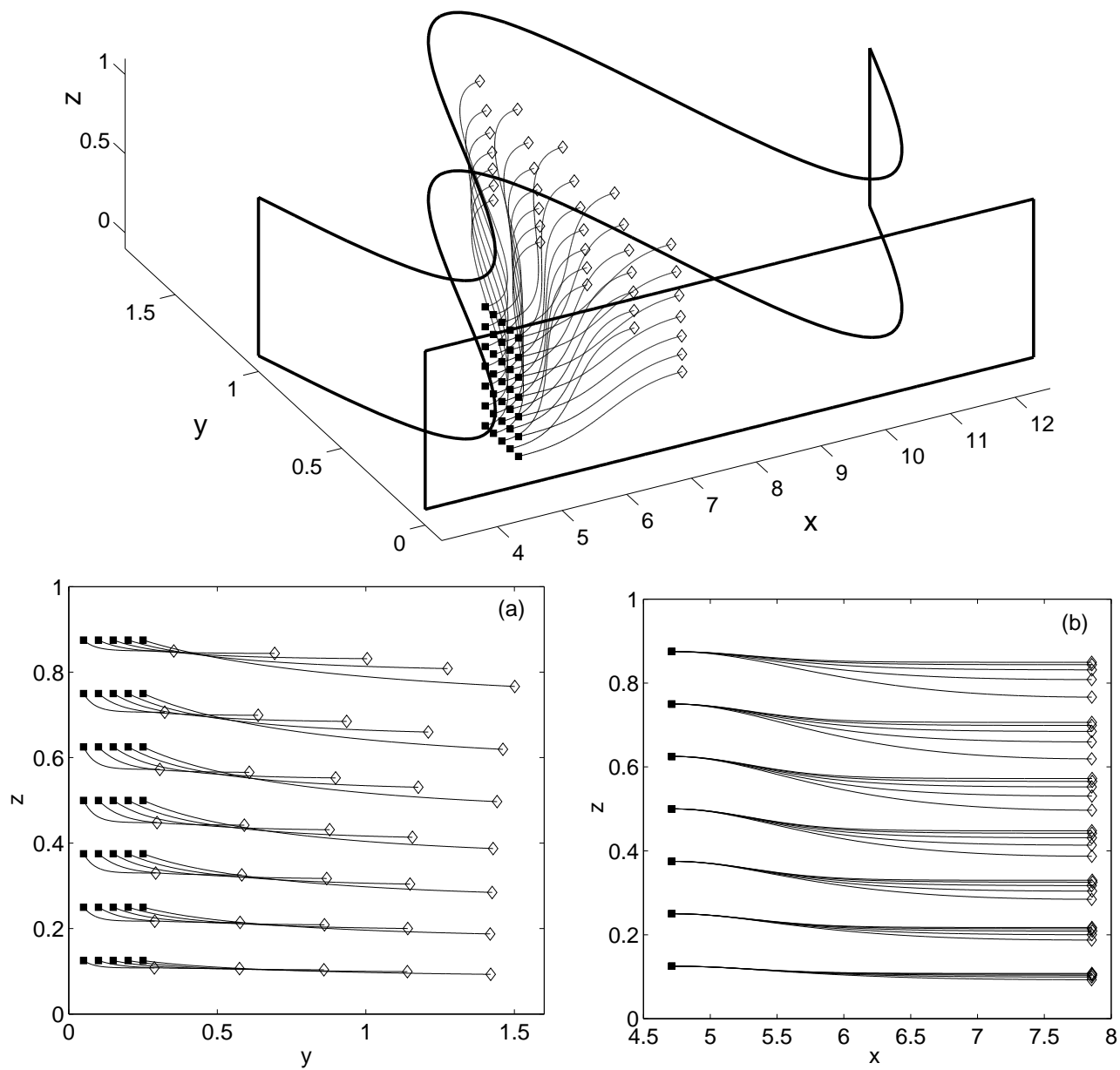


FIG. 5: Three-dimensional leading-order streamlines in the planar channel of varying dimensionless cross-section given by  $f(x) = 1 + 0.7 \sin x$ . The channel is the same as the one illustrated in Figure 4 and only the streamlines in the quadrant ( $y > 0, z > 0$ ) are reported; those in the other quadrants can be found using the flow symmetries (42). The dimensionless time step used for computation is 0.025 and 35 initially evenly spaced streamlines are considered. Top: three-dimensional view of the streamlines between the location of minimum width  $x = 3\pi/2$  (squares, filled) and the location of maximum width  $x = 5\pi/2$  (diamonds); the channel boundary and centerplane are also displayed. Bottom: (a) projection of the streamlines onto the  $(y, z)$  plane; (b) projection of the streamlines onto the  $(x, z)$  plane.

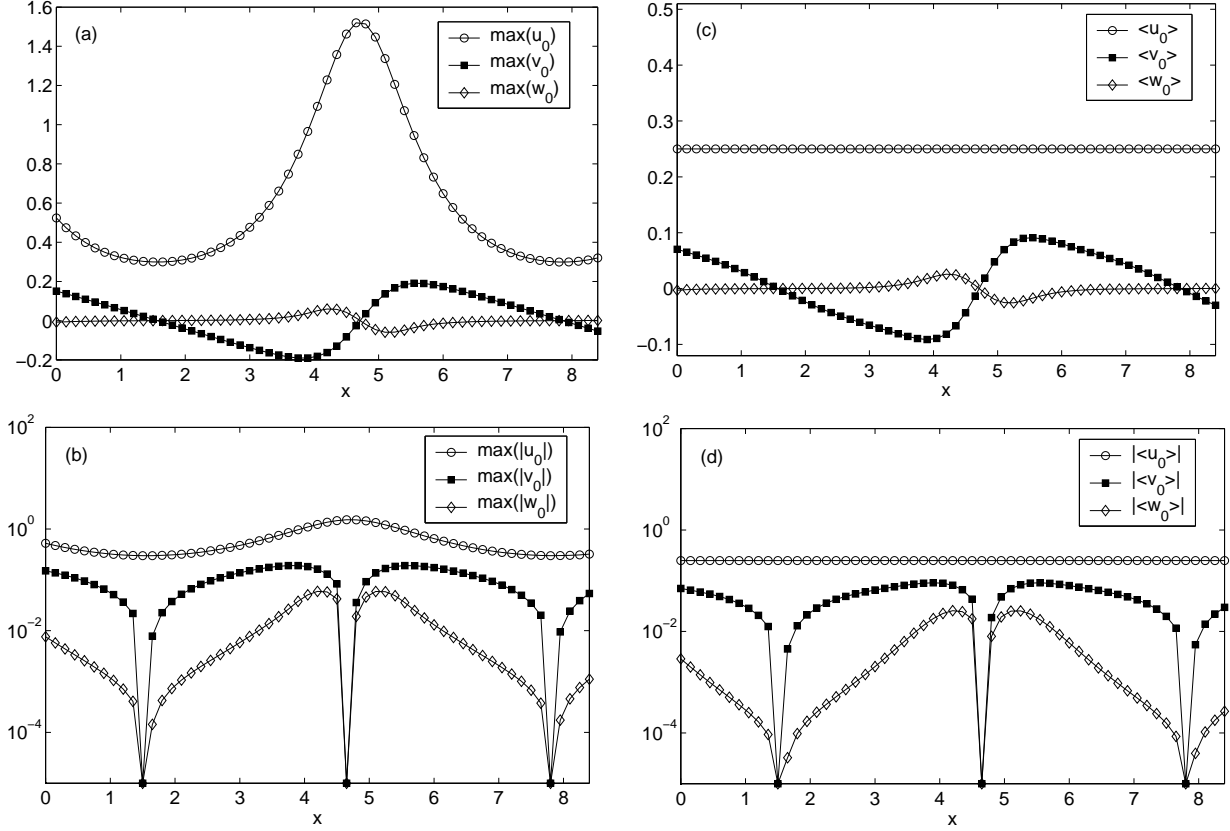


FIG. 6: Illustration of the leading-order three-dimensional flow strength in the planar channel of varying dimensionless cross-section  $f(x) = 1 + 0.7 \sin x$ . The channel is the same as the one illustrated in Figure 4 and only the velocities in the quadrant ( $y > 0, z > 0$ ) are considered. Figures (a) and (b): maximum cross-sectional values of the three components of the leading-order dimensionless velocity along the channel  $u_0$  (circles),  $v_0$  (squares, filled) and  $w_0$  (triangles); (a): regular scale, (b): semi-log scale; note that when  $v_0$  and  $w_0$  were found to be zero, which happens at each location along the channel where  $f'(x) = 0$  under the lubrication approximation, they were replaced by  $10^{-5}$  for the semi-log figures. Figures (c) and (d): same as in (a) and (b) for the quadrant-averaged velocities  $\langle u_0 \rangle$ ,  $\langle v_0 \rangle$  and  $\langle w_0 \rangle$ ; (c): regular scale, (d): semi-log scale.

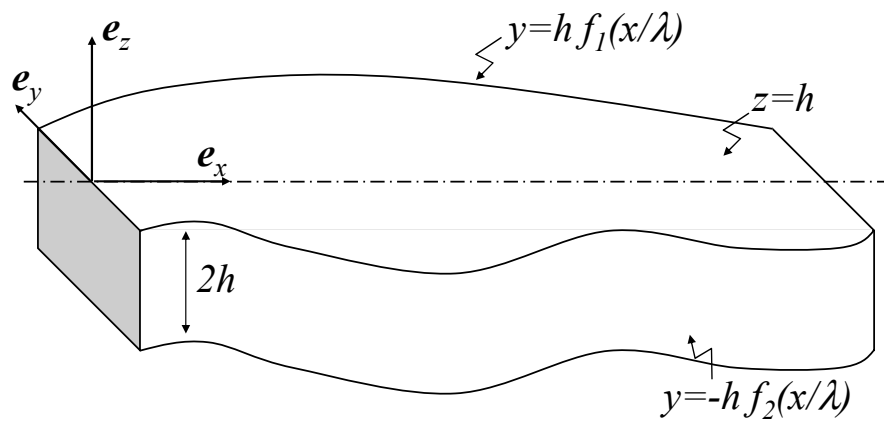


FIG. 7: General shape of a (asymmetric) planar channel.